OPEN ACCESS
IOP Publishing
Environmental Research Letters
Environ. Res. Lett. **9** (2014) 035002 (9pp)
doi:10.1088/1748-9326/9/3/035002

Flood extent mapping for Namibia using change detection and thresholding with SAR

Stephanie Long[1], Temilola E Fatoyinbo[2] and Frederick Policelli[3]

[1] Department of Earth and Environment, Florida International University, Miami, FL, USA
[2] Biospheric Sciences Laboratory, Code 618, NASA Goddard Space Flight Center, Greenbelt, MD, USA
[3] Office of Applied Sciences, Code 610, NASA Goddard Space Flight Center, Greenbelt, MD, USA

E-mail: stephanie.long@fiu.edu

Received 11 September 2013, revised 13 December 2013
Accepted for publication 10 January 2014
Published 11 March 2014

Abstract

A new method for flood detection change detection and thresholding (CDAT) was used with synthetic aperture radar (SAR) imagery to delineate the extent of flooding for the Chobe floodplain in the Caprivi region of Namibia. This region experiences annual seasonal flooding and has seen a recent renewal of severe flooding after a long dry period in the 1990s. Flooding in this area has caused loss of life and livelihoods for the surrounding communities and has caught the attention of disaster relief agencies. There is a need for flood extent mapping techniques that can be used to process images quickly, providing near real-time flooding information to relief agencies. ENVISAT/ASAR and Radarsat-2 images were acquired for several flooding seasons from February 2008 to March 2013. The CDAT method was used to determine flooding from these images and includes the use of image subtraction, decision-based classification with threshold values, and segmentation of SAR images. The total extent of flooding determined for 2009, 2011 and 2012 was about 542 km^2, 720 km^2, and 673 km^2 respectively. Pixels determined to be flooded in vegetation were typically <0.5% of the entire scene, with the exception of 2009 where the detection of flooding in vegetation was much greater (almost one third of the total flooded area). The time to maximum flooding for the 2013 flood season was determined to be about 27 days. Landsat water classification was used to compare the results from the new CDAT with SAR method; the results show good spatial agreement with Landsat scenes.

Keywords: flooding, SAR, remote sensing

1. Introduction

It is estimated that one billion people live in extreme flood areas, a number which may double by 2050 in the face of climate change and population increase (Bogardi 2004). Knowledge of the spatial extent of extreme flooding is an asset to decision makers and disaster relief agencies aiming to efficiently provide immediate and lasting support to those populations affected by flood events.

The Chobe floodplain, a seasonal marshland in the upper Zambezi River basin in Southern Africa was selected for this study in response to the recent advent of extreme flood seasons beginning in March of 2009. Zambia, Namibia, Botswana, and Zimbabwe share wetlands and tributaries in the upper Zambezi river basin (Beilfuss 2012) and have been affected by the flood events through the displacement of people, loss of crops and property, and even deaths (Inambao 2009, IRIN 2009, IFRC 2011). Disaster relief agencies have need for quick response or near real-time flood extent maps of this region to provide

service to inundated areas. Additionally, any regional planning may benefit from accurate and current flood extent maps.

Pricope (2013) has evaluated flood dynamics of the Chobe floodplain for the period of 2000–2010, using AVHRR NDVI, MODIS NDVI and EVI, and Landsat NDWI for analysis of flood extent. However, the use of optical sensors is often unreliable due to the spectral similarities between burned areas and flooded areas (Pricope 2013), the lack of available cloud-free images (Biggin and Blyth 1996), and the inability to detect standing water in vegetation (Townsend and Walsh 1998). Synthetic aperture radar (SAR) provides an all-weather, all-day tool for imaging flood events at near real-time. SAR sensors are able to detect flooding because flat surfaces reflect the signal away from the sensor, decreasing the amount of returned radiation (Gan *et al* 2012). SAR may also be used to detect flooding in vegetated or urban areas due to the brightening effects caused by the signal's double-bounce off of objects in standing water (Hess *et al* 1990, Schumann *et al* 2010, Mason *et al* 2011).

SAR-based techniques for flood detection include histogram thresholding or clustering (Inglada and Mercier 2007, Martinis *et al* 2009), radiometric thresholding (Matgen *et al* 2011), the application of neural networks in a grid system (Kussul *et al* 2008), fractal dimensioning of multi-temporal images (Huang *et al.* 2011), pixel-based segmentation (Martinis *et al* 2009), and statistical active contouring (Horritt *et al* 2001). While most methods use a single image to process the flood event, change detection can be used to provide reference brightness information (Inglada and Mercier 2007, Huang *et al* 2011, Gan *et al* 2012) and works well in coordination with other techniques such as histogram thresholding and segmentation. Some methods rely on high-resolution topography for analysis (Townsend and Walsh 1998, Schumann *et al* 2007, Mason *et al* 2011, Gala and Melesse 2012); however, accessibility to this information for remote areas of the world may be impossible. Moreover, elevation based methods for delineating floodplains or drainage areas are not effective in semi-arid regions with porous sandy soils and low topographic gradients (Pricope 2013).

Most SAR-based techniques for flood detection have been developed for monitoring large river flooding in the temperate northern latitudes; including the UK (Martinis *et al* 2009, Horritt *et al* 2001), Germany (Henry *et al* 2006) and eastern Europe (Gan *et al* 2012). However, few studies have focused on flooding in areas such as sub-Saharan Africa and the Zambezi River basin where seasonal flooding is common, yet intense periods of drought can change the landscape.

The development of a flood detection method for the Chobe floodplain must be able to operate independently of inaccessible ground-truth data such as river water levels, high-resolution topography, river delineations, and vegetation coverage. Additionally, flooding in vegetation must be identifiable as the floodplain can be highly vegetated in the permanent marshland areas. Finally, an operational flood detection network may rely on a range of sensors onboard various available satellites to capture floods in near real-time resulting in different viewing geometries, incidence angles and resolution on the ground; therefore, the procedure for flood detection must be standardized for a variety of SAR sensors Based on these requirements and the available techniques, a method of change detection and thresholding in coordination with adaptive filtering and segmentation (change detection and thresholding, CDAT) was developed for this region. The CDAT method was applied to determine the extent of inundation during seasonal flood events in Caprivi, Namibia in 2009, 2011, 2012, and 2013 using available images from ENVISAT/ASAR and Radarsat-2 SAR sensors.

2. Site description

The upper Zambezi basin receives over 37 000 million cubic meters of runoff from the surrounding 515 000 km^2 of Nambia and Zambia (Beilfuss 2012). The Chobe floodplain is located at the outfall of this basin, providing a large wetlands area and increasing the evapotranspiration of the river. Seasonal flooding is critical to the health and productivity of this area, and in recent years has increased causing the re-emergence of perennial lakes and wetlands which had dried up considerably since the 1980–1990 dry period.

At almost 2600 km in length, the Zambezi is the largest river in southern Africa, with a catchment area that covers eight countries (Moore *et al* 2007). The river and its tributaries feature waterfalls, floodplains, lakes, gorges, and now hydroelectric dams. Today the river is important as a fishery, for use in irrigation, for hydropower, and as a sanctuary for a diverse array of wildlife, which also attracts eco-tourism (Shela 2000).

Despite the large amount of rainfall that the area receives, averaging about 990 mm yr^{-1} for the entire catchment, the majority of the rainfall arrives in less than 6 months with the remainder of the year in drought. In addition to the temporal polarity of precipitation, some areas of the Zambezi experience far less than the total basin average; the Kwando/Chobe sub-catchment area which feeds the Chobe floodplain and the upper Zambezi only receives about 800 mm/year of rainfall whereas the headwaters of the Zambezi receives about 1330 mm/year on average (Beilfuss 2012). The Zambezi basin has experienced severe or persistent droughts as recent as the 1980s and 1990s, which represented some of the most severe droughts since the 1915–1935 drought period (Shela 2000).

When the rain does arrive, the extended periods of drought combined with the large flux of rainfall can lead to large amounts of runoff and flooding. In March 2009, the upper Zambezi swelled over its banks and flooded portions of Zambia and Namibia, claiming lives and destroying property. The Caprivi and Kavango regions were among the hardest hit; the Zambezi water level had reached its highest level recorded since 1969 (IRIN 2009, Bosch 2011). In the Caprivi region, lake Liambezi received floodwaters from the Zambezi via the Bukalo channel, replenishing the area and threatening unprepared communities after being largely dried up since the 1990s (Inambao 2009).

Again in 2010, the Zambezi flooded into the Caprivi region affecting over 100 000 people and damaging infrastructure, field crops and livestock (IFRC 2011). In January of 2013, the Zambezi water levels began to rise again, reaching

Table 1. List of evaluated SAR images, reference images are highlighted.

Satellite/sensor	Image date	Beam mode	Resolution (m)
ENVISAT/ASAR	26 February 2008	WSM	6×77
ENVISAT/ASAR	20 March 2009	WSM	60×77
Radarsat-2/SAR	16 March 2011	S5	12.5
Radarsat-2/SAR	17 February 2012	F0W3	6.25
Radarsat-2/SAR	29 April 2012	F0W3	6.25
Radarsat-2/SAR	30 January 2013	F6	6.25
Radarsat-2/SAR	8 February 2013	S1	12.5
Radarsat-2/SAR	11 February 2013	F4N	6.25
Radarsat-2/SAR	5 March 2013	F1N	6.25
Radarsat-2/SAR	7 March 2013	F3F	6.25
Radarsat-2/SAR	12 March 2013	F3F	6.25

6.31 m in the Caprivi region, the highest levels ever on record for January (IFRC 2013).

The mechanism for flooding into the Caprivi region is due to the Chobe River and its floodplain. During normal flow regimes, the Chobe River acts as a tributary for the Zambezi. However, during flood events the Chobe river reverses direction and flows back into the floodplain, inundating up to 1700 km^2 (Beilfuss 2012).

The intensity of the annual flood is cyclic, showing periods of above average high water levels and periods below average (Moore *et al* 2007, Beilfuss 2012, Mazvimavi and Wolski 2006). Mazvimavi and Wolski (2006) have concluded that there is an underlying multi-decadal cycle (of unknown origin) which drives these changes in seasonal flows in the Zambezi River. Their cycle study also showed that the Zambezi should be moving towards a period of high-flow; a notion that is supported by the resurgence of large flood events in the Upper Zambezi over the last 5–10 years However, Pricope (2013) has documented a general decrease in the overall flooding of the region since 2000 based on evaluation of optical flood detection methods.

3. Data and methods

SAR images include two ENVISAT/ASAR images taken 26 February 2008 and 20 March 2009. Additionally, Radarsat-2 images taken from 27 February 2011 to 12 March 2013 were acquired. Table 1 lists the images that were processed for this study; the images used as a reference are shaded (note that the 17 February 2012 image was used as a reference for both the 2011 and 2012 flood events). All SAR images were of HH polarization; this is the preferred polarization for flood extent mapping because it is less sensitive to minor vertical differences on the water surface caused by waves (Henry *et al* 2006, Martinis *et al* 2009, Gan *et al* 2012).

3.1. Image preprocessing

All SAR images were georeferenced and stacked using ENVI software in order to perform a change detection process. The adaptive Gamma (maximum *a posteriori*—MAP) filter produces speckle-removed images with relatively low processing time (Lopes *et al* 1990, Martinis *et al* 2009). This method was ultimately selected for speckle removal, as it was effective for all of the available SAR resolutions, angles, and sensor modes. The images were processed with a Gamma filter over a 5×5 window with 2 looks.

The CDAT method was used to process recent seasonal flood events in the Chobe flooplain from 2009 to 2013. The images were georeferenced, filtered with the adaptive Gamma filter and masked. Figure 2 shows the pre-processed imaged from 2012 and 2011, the Gamma filter removed speckle and smoothed the image. The dark portions of the image represent flat surfaces such as water.

3.2. Change detection and thresholding (CDAT)

Two images were selected to evaluate the flood extent, one reference image and one 'flooded' image from after the storm event. The following method was then applied to extract the flood extent from the two images:

(1) Band math—difference of the absolute values of the images.

(2) Thresholding—classify pixels of the difference image, which are dark as flooded or very bright as flooded in vegetation, based on threshold criteria.

(3) Segmentation—group larger areas of flooding.

A difference expression was applied on the stacked images to get the absolute difference (D) between the reference image (R) and the flooded image (F)

$$D = |\text{float(F)}| - |\text{float(R)}|. \quad (1)$$

The result of the band math is the differenced image. Areas that were darker in the flooded image appear dark in the difference image, while areas that were dark in both images appear gray indicating no change. The differenced image is then masked to set any edges or overlay errors to zero before classification.

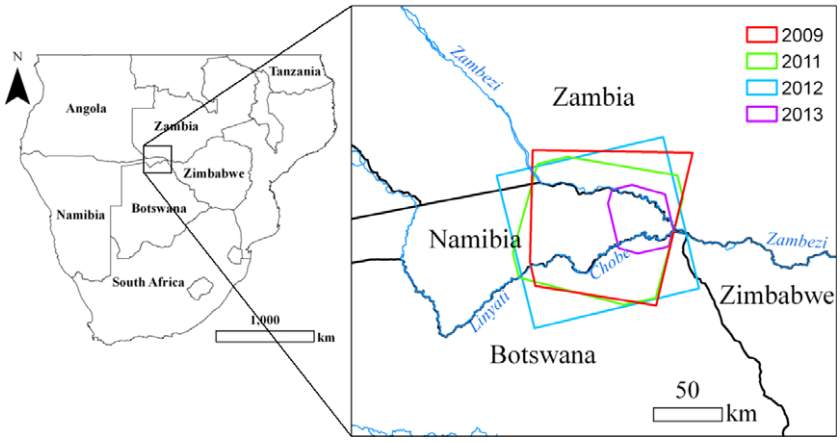

Figure 1. Location map with SAR image outlines for 2009 (red), 2011 (green), 2012 (light blue), and 2013 (magenta).

3.2.1. Thresholding. Histogram thresholding involves separating the image into several gray scale ranges based on peaks in the histogram (Deshmukh and Shinde 2005). A threshold value was determined from the valleys in between two peaks.

The thresholding process was applied using a decision tree classification. The decision tree starts with a masking decision, which asks if the pixel of the differenced image (P_D) has a slope less than 3° by analyzing the slope of the input digital elevation model (DEM). This step masks these steeper slopes and therefore removes any pixels in the SAR image that may show a change in brightness due to the angle of signal return from hills and slopes (Hess *et al* 1990). The removal of these bright pixels is important for calculation of the local statistics during thresholding; however, this step may be unnecessary and therefore omitted for regions with relatively flat topography. A slope of 3° was chosen as a conservative standard slope, and includes areas such as steep river banks, hydraulic structures, and hill slopes. The SRTM global digital elevation model for Africa was acquired from the USGS online resource and was used for all SAR imagery. Since this is a global DEM it can be used for other regions around the world.

Another step masks any background pixels which were set to zero in the differenced image using the masks for each year as shown in figure 1. The sloped pixels and the zero-value background pixels are classified as Class 0.

Surviving pixels were evaluated for flooding using the brightness variance to set the threshold criteria. In the case of flooded pixels, the threshold criterion is simply that the pixel is less than the mean pixel value minus the standard deviation of the entire image times a coefficient k_f. The following criterion determines if the pixel (P_D) is inundated:

$$P_D < (\{\text{lmean}[D]\} - k_f * \{\text{lstdev}[D]\}) \quad (2)$$

where lmean is the mean of the surviving pixels and lstdev is the standard deviation of the surviving pixels. The optimal value of k_f was determined to be 1.5 for this region based on several iterations. Several criteria are examined during the calibration of the k_f value; including amount of remaining speckle and its coverage, visual correlation to Landsat imagery and aerial photographs, and identification of characteristic flooding patterns (i.e. proximity to rivers and inundation of dry streambeds).

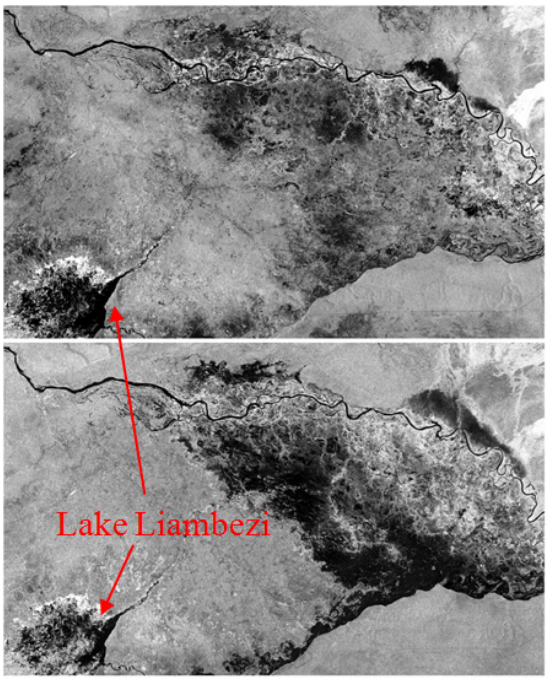

Figure 2. Example of pre-processed Radarsat-2 SAR images taken pre-flood (top) and post-flood (bottom). Darkened areas are associated with flooding. Lake Liambezi is indicated at the bottom left.

If the inundation criterion is not met, the pixel is then evaluated for flooding in vegetated or urban areas using the brightness variance and a multiplicative coefficient to determine the threshold criteria. In the case of flooding in vegetated areas, the threshold criterion is that the pixel is greater than the mean pixel value minus the standard deviation times some coefficient k_{fv}. The following criterion determines if the pixel is inundated in a vegetated area:

$$P_D > (\{\text{lmean}[D]\} + k_{fv} * \{\text{lstdev}[D]\}). \quad (3)$$

The optimal value of k_{fv} was determined to be 2.5 for this region using the same method as for the value of k_f.

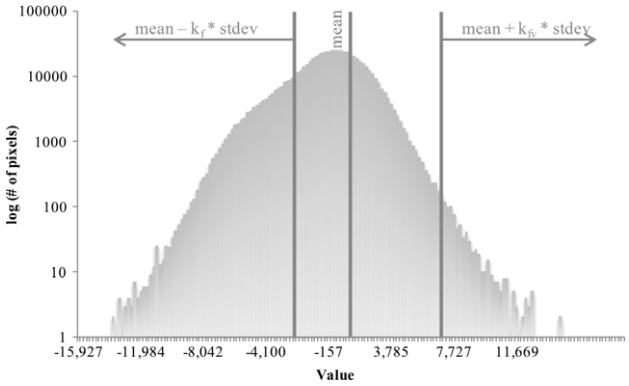

Figure 3. Histogram of the 2011 differenced image showing the mean and flooding ranges.

The threshold coefficients showed sensitivity to the scale of the image and extent of flooding. For example, the 12 March 2013 image was small in scale and almost the entire image was flooded resulting in a lower local mean of the image and smaller local standard deviation, which could have caused an overestimation of flooded pixels.

A log scale histogram of the 2011-differenced image is shown in figure 3. Ignoring background values, the range of the flooded images relies on the mean and standard deviation of the pixel values of the entire image In the 2011 differenced image the majority of the pixels are unchanged (near zero), representing normal river boundaries and land cover unaffected by flood. The peak in the number of pixels below the mean represents the large population of flooded pixels.

SAR image brightness depends on incidence angle of the sensor during acquisition (Gan *et al* 2012). However, this method relies on statistical relationships of the differenced values, eliminating the need to retain the explicit brightness values. This means that SAR scenes with different incidence angles can be used to evaluate flooding without issue.

3.2.2. Segmentation and extraction. The ENVI Segmentation tool clusters classified pixels into groups of the same class type, and puts the data in a raster format with separate object ID's for each grouping. Segmentation is a useful postprocessing tool for radar because of the minimum pixel requirement for the groupings, ignoring sporadic bright or dark pixels associated with image speckle that were missed by the preprocessing. It also grows flooded regions by connecting groups based on neighboring pixel classifications. Segmentation was performed separately for Class 2 (Flood) and Class 3 (Flood in Vegetation). The tool groups pixels based on the number of neighboring pixels (4 or 8) and the minimum number of pixels per group. While many combination options were examined, better results were found (i.e. less speckle and flooded feature retention) when neighboring groups were larger (8 neighbors) and the number of pixels per group was smaller (a minimum of 30). This way, denser groups of flooded pixels and smaller flooded features could be identified among the speckle.

Table 2. Total area of flooding increase for each evaluated year and percent of total flooding that is considered flooding in vegetation.

Flood year	2009	2011	2012	2013
Total flooded area (km^2)	541.69	719.71	673.22	551.38
Percent as flooding in vegetation (%)	30.68	5.83	12.27	1.05

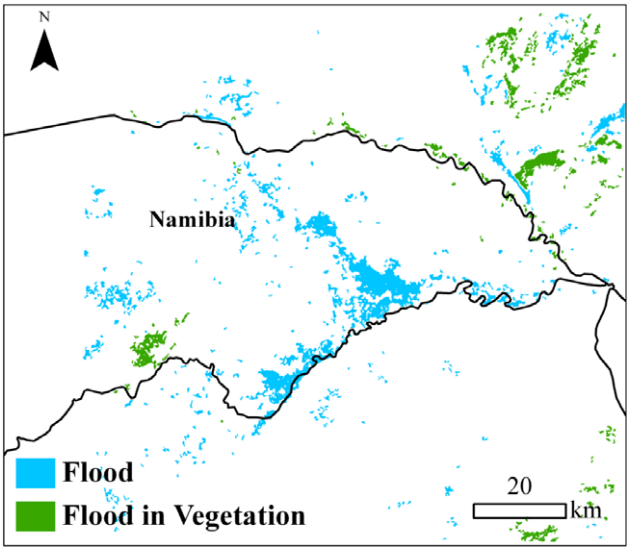

Figure 4. The 2009 flood extent (blue) and flooding in vegetation (green) using the CDAT method with ASAR images.

4. Results and discussion

4.1. Flood extent of the Chobe floodplain

Table 2 shows the total area of flooding increase for each evaluated flood event. The 2011 event showed the largest flood extent (about 720 km^2) and the 2009 event had the smallest extent (about 540 km^2). The 2013 flood event showed the least amount of flooding in vegetation (about 1% of the total flooding), which may be a result of the finer resolution of the SAR image.

The 2009 flood event was evaluated with available ENVISAT/ASAR images from 26 February 2008 and 20 March 2009. Figure 4 shows the flood extent in blue (for open water) and green (for flooding in vegetated areas). The extent of flooding evaluated is only illustrating the increase in flood extent from the previous year and not the entire extent. It should also be noted that the flood in 2009 continued to expand even after the image was captured on 20 March 2009.

Of the images available, the most appropriate reference SAR image for the 2011/2012 period was 16 February 2012 due to the relative 'dryness' of the floodplain. This image was used to process the 2011 and 2012 flood events with the CDAT method. Results show excellent spatial correlation to the actual flooded areas.

Figure 5 shows the 2011 flood extent as determined by the CDAT with SAR method. The flood event was captured by Radarsat-2 on 16 March 2011 and compared to the 16

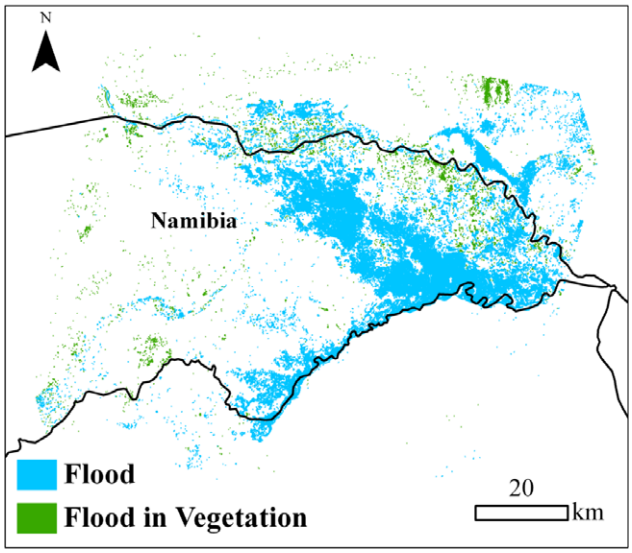

Figure 5. The 2011 flood extent (blue) and flooding in vegetation (green), extracted using the CDAT method with Radarsat-2 images.

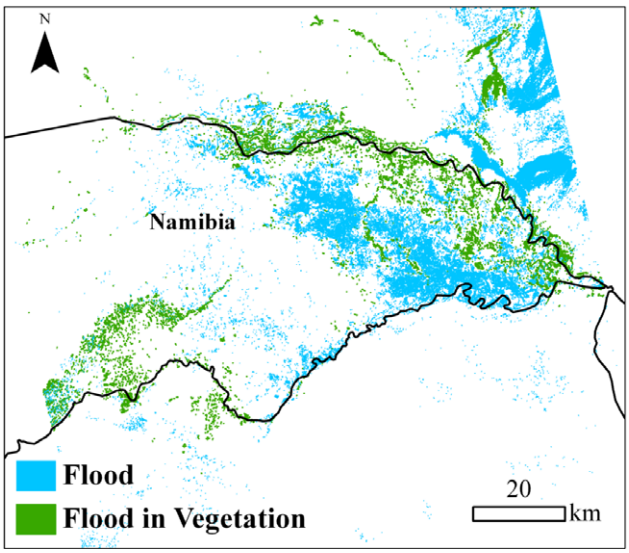

Figure 6. The 2012 flood extent (blue) and flooding in vegetation (green) using the CDAT method with Radarsat-2 images.

February 2012 image. Shown in figure 6 is the 2012 flood extent as determined by the CDAT with Radarsat-2 method for 29 April 2012 as compared to the 16 February 2012 image. Flood extents from 2011 and 2012 are similar; however, flooding along the Chobe River is more extensive in 2011. Both maps show flooding in vegetation along the Zambezi and its marshland or delta. In addition, both maps captured some swelling of lake Liambezi near the Linyati River. This appears flooded near the banks of the lake in 2011 and flooded in vegetation in 2012, possibly indicating land cover change.

4.2. Time to flood

The extent of flooding between 30 January 2013 and 12 March 2013 was determined from the CDAT with Radarsat-2 images. Several SAR images were available for the 2013 flood in the Chobe floodplain, beginning from the start of the flood season on 30 January 2013 and ending on 12 March 2013 (see table 1 for a list of available images). The images were from Radarsat-2 and were taken using Fine beam mode or wide fine beam mode, with the exception of the 4 February image taken in Standard mode. The images were all resampled to 12.5 m × 12.5 m resolution and smoothed using the adaptive Gamma filter.

The time to maximum flood extent is very rapid in the Chobe Floodplain, depending on the season. A time series of SAR images for the 2013 flood season was evaluated. Figure 7 shows extent of inundation with time and figure 8 graphs the percent of inundated pixels with time. The flood extent is shown in blue and flooding in vegetation in green. The area

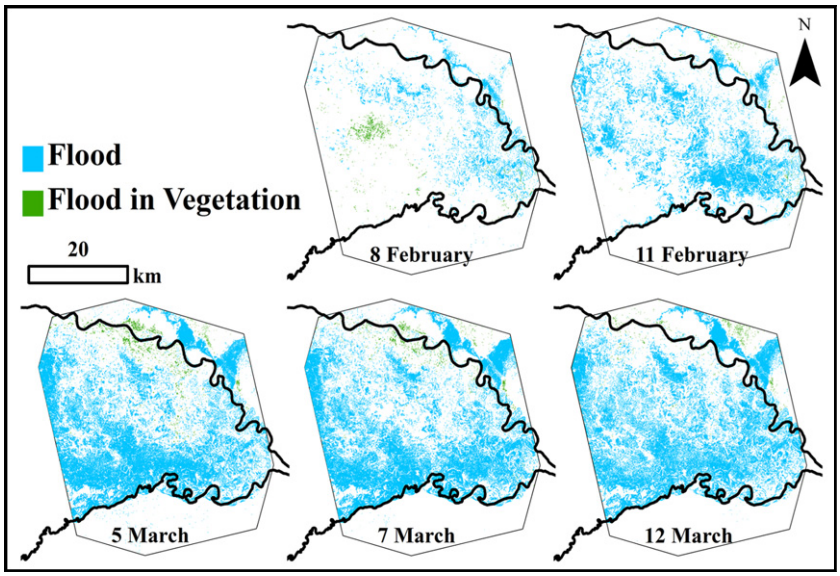

Figure 7. Flood maps from 30 January 2013 to 12 March 2013.

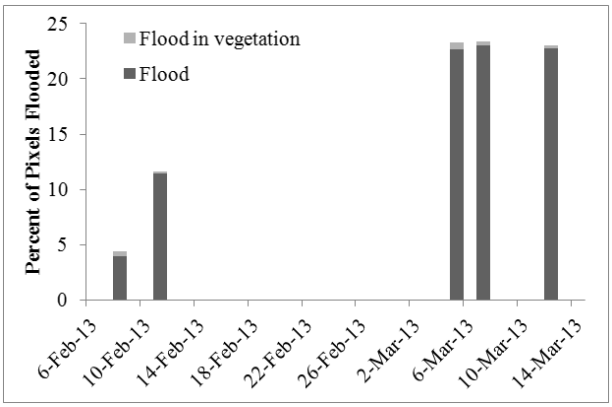

Figure 8. Percent of flooded pixels for the 2013 flood season.

available for study, as determined by the size of the available images, is outlined on the map. The flood extent maps, which are limited spatially due to the small swath of the SAR images, suggest that the full extent of flooding was reached on 7 March 2013. Since the initiation of flooding in early February, the extent of flooding changed very rapidly increasing by 20% and inundating over 550 km^2 in 27 days.

4.3. Landsat comparison

Landsat images were downloaded from the USGS EarthExplorer website (http://earthexplorer.usgs.gov/) for flood extent comparison to the CDAT with SAR method. Landsat scenes were selected based on the dates of the SAR images and scene clarity. Landsat TM, ETM+ and OLI sensors have a shortwave infrared (SWIR) band, which is useful for determining inundated regions (Gala and Melesse 2012). A density slice of the SWIR band (Band 5 for TM or ETM+) or a multi-band classification of Bands 2–6 with Landsat 8 OLI was used; both methods performed equally well for defining water extent. The flooded areas were then subtracted from the classification of a non-flooded day on about the same dates as the SAR reference images. Subtracted results were then compared to the flood extents determined using the CDAT method. Because it is difficult to determine flooding in vegetation using Landsat, this was not considered during the comparison.

The system for evaluating the pixel-based comparison includes the use of upper and lower-case letters which indicate percentage of flooded pixels ('F' for the SAR method and 'f' for the Landsat method) and non-flooded pixels ('N' for the SAR method and 'n' for the Landsat method). 'Ff' represents pixels which are considered flooded for both methods, 'Nn' are pixels which are considered non-flooded for both methods, 'Nf' are pixels which are considered non-flooded for the SAR method and flooded for the Landsat method and 'Fn' are pixels which are considered flooded for the SAR method and non-flooded for the Landsat method.

Table 3 shows the pixel-based comparison of the CDAT with SAR method and the Landsat classification. The CDAT method produced a large percentage of non-matching pixels (Nf plus Fn) due in large part to the cloudiness of the Landsat scenes, difference in time of acquisition for the

Table 3. Pixel-based comparison of Landsat and SAR methods for three flood events. Shown are the percentages of pixels marked as Ff (flooded for both methods), Nn (non-flooded for both methods), Fn (flooded for the SAR method only), or Nf (flooded for the Landsat method only).

Flooding year	2009	2011	2013
Ff (both flooded)	0.88	4.50	7.24
Nn (both non-flooded)	90.80	84.20	69.87
Fn (SAR flooded)	2.47	0.82	15.52
Nf (landsat flooded)	5.86	10.48	7.37
Total non-matching pixels	8.32	11.30	22.89

Landsat and SAR images, image resolution, and method of flood extent detection. For all three evaluated years, 30–90% of the total non-matching pixels came from areas marked non-flooded in the SAR images yet are considered flooded by Landsat classification due to darkening by cloud shadow in the Landsat scene, additional land cover changes occurring between Landsat scenes, or because the flood extent increased in the moments between the SAR and Landsat acquisition. One exception is the 2013 flood year, which showed a greater number of flooded pixels in the SAR image. This may be due to the improved ability of the CDAT with SAR method to capture flooded areas, as much of the Landsat scene has emergent vegetation which can be erroneously classified as non-flooded.

The percentage of pixels in error (or non-matching) increased with the increasing resolution of the SAR images. For the 2009 flood, the method was tested using ENVISAT/ASAR images with 60 m resolution, the 2011 flood event was imaged with Radarsat-2 with a resolution of 12.5 m, and the 2013 images have a raw resolution of 6.25 m. The increasing resolution (from 60 to 6.25 m) results in increasingly detailed outlines of inundated areas and may allow for inundated area separation due to SAR speckle.

Despite the large pixel error, the maximum spatial extent of flooding corresponds well with that of the Landsat scenes. For the 2009 flood extent, much of the flooded area matches up well on visual inspection with a Landsat 5 TM scene from the following month. However, the Landsat image is marred by clouds; a common optical problem which does not affect SAR imagery. The ability to acquire images despite cloud cover or time of day gives the CDAT with SAR method a clear advantage over optical methods, such as classification with Landsat.

It is with caution that we compare two image acquisitions, two sets of differenced images, even two images from different imaging modes; but it is with particular caution that we compare two different physical means of obtaining land surface information (optical and radar). Townsend and Walsh (1998) found Landsat TM data to be a poor indicator of flooding, especially during periods of 'leaf-on'. They concluded that SAR images are superior to optical for determining flooded pixels (Townsend and Walsh 1998). However, there are few other options for ground-truthing in this remote region of the world and Landsat, which is free and publicly accessible, can be used for visual inspection.

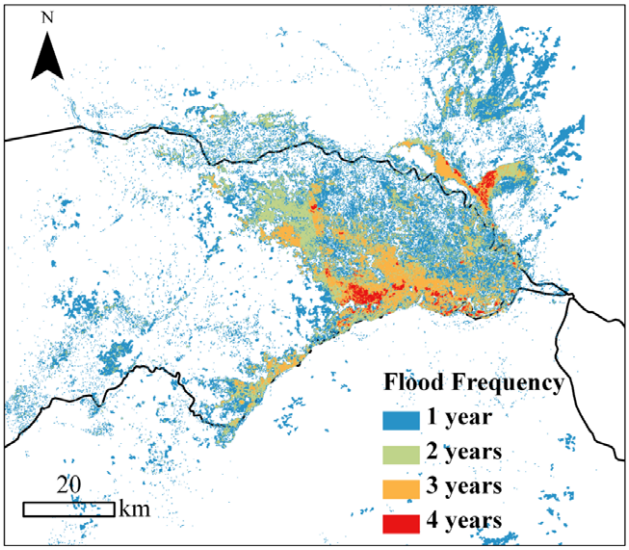

Figure 9. Frequency of total flooding for 4 seasons (2009 and 2011–2013).

4.4. Flooding frequency

Figure 9 spatially illustrates the frequency with which flooding occurs. This indicates potential extent of seasonal flooding. In figure 9, areas in red and orange have been flooded more frequently from 2009 to 2013 and represent a certainty of flooding for future flood seasons. In all four years, 22% of flooded pixels have flooded at least twice (either open flooding or flooding in vegetation) and 9.8% have flooded at least three times.

5. Conclusion

Recent flooding was evaluated in the Chobe floodplain in the Caprivi region of Namibia using a novel change detection and thresholding technique, the CDAT method, with SAR images from ENVISAT/ASAR and Radarsat-2. The method uses threshold values based on the statistics of each set of differenced SAR images, allowing an individualized estimation of flooding. The straightforwardness of the difference and classification method allows for future automation for near real-time flood extent mapping. The CDAT method is novel in that it utilizes statistical thresholding techniques *after* the images are subtracted. This process provides the extent of additional flooding, and eliminates the need for detailed floodplain or river bank delineations, which may change over time and can be difficult to obtain for remote regions of the world.

The 2009 Chobe flood was compared with the less intense 2008 flood and showed an increase of inundation of about 542 km^2. The flood was recognized as a disaster by relief agencies mainly because it caused a re-emergence of perennial wetlands, which were dry for 13 years and had been claimed as farmland in that time. Many were displaced by the flood, experienced property damage or loss, or were threatened by the loss of food security (IRIN 2009). The 2009 flood extent maps created using the CDAT with ASAR showed good correlation to the 2009 Landsat classification both spatially and on a pixel-based comparison.

The 2011 and 2012 flood events in March and April were evaluated with a relatively dry image from 17 February 2012 as the reference. These flood extent maps illustrate the full extent of inundation (720 km^2 in 2011 and 673 km^2 in 2012) including flooding in vegetated areas along river banks and around wetlands. The 2011 flood extent map showed good correlation to the Landsat flood extent classification; however, the difference of image acquisition dates and cloudiness of the Landsat images caused moderate pixel error during comparison.

Although the pixel error was high for 2013, the inundation extent was spatially similar to that of the Landsat classification. Because several Radarsat-2 images were available, the flood event was tracked with time revealing a relatively fast speed of inundation (27 days to flood about 550 km^2). The speed and pattern with which the wetland floods are important to evaluate as it is rapid flooding in unprepared regions which can be the most devastating and destructive. This method can also be used to evaluate drainage rates in this region, allowing communities and relief agencies to plan accordingly.

One restriction of this method is the date of acquisitions of the reference image. Reference images provide knowledge of the 'dry' or non-flooded scenes, and have great weight in the analysis of the flood extents. When a reference image is also flooded, as is the case of the 2009 flood analysis, the resulting flood extent map is actually illustrating the extent of *additional* flooding and should be clarified. SAR imagery can also be expensive (depending on the satellite, sensor type, or image resolution) or coverage may be absent, making it difficult to obtain a new reference image. This restriction is easily controlled when there is understanding of the hydrology of the region prior to image acquisition.

The use of SAR imagery has proven useful for a variety of flood extent mapping methods (Gala and Melesse 2012, Gan *et al* 2012, Hess *et al* 1990, Inglada and Mercier 2007, Townsend and Walsh 1998). The CDAT method was developed based on the use of SAR due to the rapid image acquisitions, consistency of imagery (day/night and all-weather) and ease of processing (one band). This technique has been successful at mapping the extents of seasonal floods in Caprivi, Namibia in 2009, 2011, 2012 and 2013 and answers the work of Pricope (2013) with more accurate flood extent analysis.

Acknowledgments

This work is supported by the NASA Earth Science Research Program through the 'Science of Terra and Aqua' solicitation, NNH09ZDA001N-TERRAQUA. The authors wish to thank the Canadian Space Agency and the European Space Agency for providing RADARSAT and ASAR radar data. The authors also thank Stuart Frye (SGT, Inc.) for his tireless work coordinating data acquisitions and data access for this work.

References

Beilfuss R 2012 A risky climate for southern African hydro: assessing hydrological risks and consequences for Zambezi River Basin dams (Berkeley, CA: International Rivers) p 56

Biggin D S and Blyth K 1996 A comparison of ERS-1 satellite radar and aerial photography for river flood mapping *J. Chartered Inst. Water Env. Man.* **10** 59–64

Bogardi J 2004 Two Billion will be in Flood Path by 2050, http://archive.unu.edu/update/archive/issue32_2.htm Update (online, accessed 28 July 2011)

Bosch N 2011 *Flooding Caprivi Namibia* (www.caprivi.biz/flooding.html, 3 July 2013)

Deshmukh K S and Shinde G N 2005 An adaptive color image segmentation *Electron. Lett. Comput. Vis. Image Anal.* **5** 12–23

Gala T S and Melesse A M 2012 Monitoring prairie wet area with an integrated LANDSAT ETM+, RADARSAT-1 SAR and ancillary data from LIDAR *Catena* **95** 12–23

Gan T Y, Zunic F, Kuo C-C and Strobl T 2012 Flood mapping of Danube River at Romania using single and multi-date ERS2-SAR images *Int. J. Appl. Earth Obs. Geoinform.* **18** 69–81

Henry J-B, Chastanet P, Fellah K and Desnos Y-L 2006 Envisat multi-polarized ASAR data for flood mapping *Int. J. Remote Sens.* **27** 1921–9

Hess L L, Melack J M and Simonett D S 1990 Radar detection of flooding beneath the forest canopy: a review *Int. J. Remote Sens.* **11:7** 1313–25

Horritt M S, Mason D C and Luckman A J 2001 Flood boundary delineation from synthetic aperture radar imagery using a statistical active contour model *Int. J. Remote Sens.* **22:13** 2489–507

Hostache R, Matgen P and Wagner W 2012 Change detection approaches for flood extent mapping: how to select the most adequate reference image from online archives? *Int. J. Appl. Earth Obs. Geoinform* **19** 205–13

Huang S, Cai X, Chen C and Liu D 2011 Change detection method based on fractal model and wavelet transform for multitemporal SAR images *Int. J. Appl. Earth Obs. Geoinform.* **13** 863–72

IFRC 2011 DREF Operation Final Report: Namibia Floods (DREF Operation No.) DRNA005 *International Federation of Red Cross and Red Crescent Societies* (reports available at: www.ifrc.org)

IFRC 2013 Disaster Relief Emergency Fund (DREF): Namibia floods (DREF Operation No.) MDRNA007 *International Federation of Red Cross and Red Crescent Societies* (reports available at: www.ifrc.org)

Inambao C 2009 *Namibia: Caprivi Floods Reach Historic Mark* (http://reliefweb.int/report/namibia/namibia-caprivi-floods-reach-historic-mark 3 July 2013)

Inglada J and Mercier G 2007 A new statistical similarity measure for change detection in multitemporal SAR images and its extension to multiscale change analysis *IEEE Trans. Geosci. Remote Sens.* **45** 1432–45

IRIN 2009 Namibia/Zambia: Food Insecurity Looms as Floods Swallow Crops *UN Office for the Coordination of Humanitarian Affairs* (www.irinnews.org/report/83623/namibia-zambia-food-insecurity-looms-as-floods-swallow-crops, 28 July 2011)

Kussul N, Shelestov A and Skakun S 2008 Grid system for flood extent extraction from satellite images *Earth Sci. Inform.* **1** 105–17

Lopes A, Nezry E, Touzi R and Laur H 1990 Maximum a posteriori speckle filtering and first order texture models in SAR images *10th Annual Int. Symp. on Geosci. and Remote Sens.* pp. 2409–12

Martinis S, Twele A and Voigt S 2009 Towards operational near real-time flood detection using a split-based automatic thresholding procedure on high resolution TerraSAR-X data *Natural Hazards Earth Syst. Sci.* **9** 303–14

Mason D C, Davenport I J, Neal J, Schumann G J-P and Bates P D 2011 Near real-time flood detection in urban and rural areas using high resolution Synthetic Aperture Radar images *IEEE Trans. Geosci. Remote Sens.* **50** 3041–52

Matgen P, Hostache R, Schumann G, Pfister L, Hoffman L and Savenije H 2011 Towards an automated SAR-based flood monitoring system: lessons learned from two case studies *Phys. Chem. Earth* **36** 241–52

Mazvimavi D and Wolski P 2006 Long-term variations of annual flows of the Okavango and Zambezi Rivers *Phys. Chem. Earth* **31** 944–51

Moore A E, Cotterill F P D, Main M P L and Williams H B 2007 The Zambezi river *Large Rivers: Geomorphology Management* ed A Gupta (Chichester: Wiley) pp 311–32

Pricope N G 2013 Variable-source flood pulsing in a semi-arid transboundary watershed: the Chobe River, Botswana and Namibia *Environ. Monit. Assess.* **185** 1883–906

Schumann G, Hostache R, Puech C, Hoffmann L, Matgen P, Pappenberger F and Pfister L 2007 High-resolution 3D flood information from radar imagery for flood hazard management *IEEE Trans. Geosci. Remote Sens.* **45** 1715–25

Schumann G J-P, Neal J C, Mason D C and Bates P D 2010 The accuracy of sequential aerial photography and SAR data for observing urban flood dynamics, a case study of the UK summer 2007 floods *Remote Sens. Environ.* **115** 2536–46

Shela O N 2000 Management of shared river basins: the case of the Zambezi River *Water Policy* **2** 65–81

Townsend P A and Walsh S J 1998 Modeling floodplain inundation using an integrated GIS with radar and optical remote sensing *Geomorphology* **21** 295–312